3-1-1993

Interatomic Forces and Atomic Structure of Grain Boundaries in Copper-Bismuth Alloys

Min Yan

Mojmír Šob
University of Pennsylvania

David E. Luzzi
University of Pennsylvania, luzzi@lrsm.upenn.edu

Vaclav Vitek
University of Pennsylvania, vitek@seas.upenn.edu

Graeme J. Ackland

See next page for additional authors

Recommended Citation
Yan, M., Šob, M., Luzzi, D. E., Vitek, V., Ackland, G. J., Methfessel, M., & Rodriguez, C. O. (1993). Interatomic Forces and Atomic Structure of Grain Boundaries in Copper-Bismuth Alloys. *Phyiscal Review B, 47* (10), 5571-5582. http://dx.doi.org/10.1103/PhysRevB.47.5571

Interatomic Forces and Atomic Structure of Grain Boundaries in Copper-Bismuth Alloys

Abstract
The many-body empirical potentials that describe atomic interactions in the copper-bismuth system were constructed using both experimental data and physical quantities obtained by *ab initio* full-potential linear muffin-tin orbital calculations for a metastable Cu_3Bi compound. These potentials were then used to calculate the structure of a grain boundary in copper containing bismuth, which was at the same time studied by high-resolution electron microscopy (HREM). Excellent agreement between the calculated and observed structures is shown by comparing a through-focal series of observed and calculated images. This agreement validates the constructed potentials, which can be used with a high confidence to investigate the structure and properties of other grain boundaries in this alloy system. Furthermore, this study shows, that HREM combined with computer modeling employing realistic empirical potentials can decipher with great accuracy the structure of boundaries containing multiple atomic species.

Disciplines
Atomic, Molecular and Optical Physics | Engineering | Materials Science and Engineering | Metallurgy | Physics

Author(s)
Min Yan, Mojmír Šob, David E. Luzzi, Vaclav Vitek, Graeme J. Ackland, M. Methfessel, and C. O. Rodriguez

Interatomic forces and atomic structure of grain boundaries in copper-bismuth alloys

Min Yan, M. Šob,* D. E. Luzzi, and V. Vitek
Department of Materials Science and Engineering, University of Pennsylvania, Philadelphia, Pennsylvania 19104

G. J. Ackland
Department of Physics, James Clerk Maxwell Building, The King's Buildings, University of Edinburgh, Edinburgh EH9 3JZ, United Kingdom

M. Methfessel† and C. O. Rodriguez‡
Max-Planck-Institut für Festkörperforschung, Heisenbergerstrasse 1, Stuttgart, Germany
(Received 1 June 1992)

The many-body empirical potentials that describe atomic interactions in the copper-bismuth system were constructed using both experimental data and physical quantities obtained by *ab initio* full-potential linear muffin-tin orbital calculations for a metastable Cu_3Bi compound. These potentials were then used to calculate the structure of a grain boundary in copper containing bismuth, which was at the same time studied by high-resolution electron microscopy (HREM). Excellent agreement between the calculated and observed structures is shown by comparing a through-focal series of observed and calculated images. This agreement validates the constructed potentials, which can be used with a high confidence to investigate the structure and properties of other grain boundaries in this alloy system. Furthermore, this study shows, that HREM combined with computer modeling employing realistic empirical potentials can decipher with great accuracy the structure of boundaries containing multiple atomic species.

I. INTRODUCTION

The atomic structure of grain boundaries in metallic materials is the key to the microscopic understanding of a wide variety of their physical and mechanical properties. This is particularly important in alloys. For example, in pure metals, with the exception of iridium,[1] grain boundaries are not susceptible to cracking. On the other hand, grain boundaries in some intermetallic compounds appear to be intrinsically brittle (see, e.g., Refs. 2 and 3), while in disordered alloys segregation of impurities and alloying elements to grain boundaries is the principal reason for grain boundary brittleness (see, for example, Ref. 4).

A very suitable model material for investigation of the segregation and embrittlement phenomena is the copper-bismuth system. Although the solubility of bismuth is rather low, it has been demonstrated that the strong intergranular embrittlement of this alloy is associated with segregation rather than precipitation of bismuth at grain boundaries.[5,6] A remarkable phenomenon observed in this system is the segregation-induced faceting[7–10] which was shown to be a reversible transformation driven by addition or removal of bismuth.[8] During aging at temperatures below 700 °C a saturation level of bismuth in grain boundaries is reached before faceting occurs and the bismuth concentration in the boundaries then remains approximately the same after faceting has fully developed.[9] This behavior changes abruptly in a very narrow range of temperatures, 700 °C–720 °C, above which desegregation occurs. This abrupt segregation-desegregation behavior cannot be explained using standard equilibrium thermodynamics theories without assuming an unreasonably large bismuth-bismuth interaction.[9] To elucidate these phenomena we need to understand the atomic structures of grain boundaries with segregated bismuth as well as the facets which develop as the result of segregation.

Until recently the principal experimental sources of information about the interfacial atomic structure were macroscopic analyses, such as the examination of intergranular fracture surfaces, and mesoscopic observations, for example, electron microscopic studies of grain boundary dislocations. For some special grain boundaries x-ray diffraction was utilized to extract more detailed structural information[11,12] but the determination of exact atomic positions is not unambiguous.

However, in the last few years, high-resolution electron microscopy (HREM) has been developing rapidly and this technique can provide direct information on the structure of material volumes of atomic dimensions. In fact, from the systematic variation of the image contrast with defocus, information on both the positions and identities of the atoms can be extracted.[13,14] Notwithstanding, an abiding interpretation of the HREM images can only be made if a physically reliable model of the studied structure is established and a direct comparison of observed images with images evaluated theoretically on the basis of this model performed. Recently, such studies have been made, for example, for boundaries in pure aluminum.[15,16] For a binary alloy such an analysis was accomplished by the present authors who investigated the structure of the $(111)/(11\bar{1})$ symmetrical tilt grain boundary corresponding to the $\Sigma=3$ misorientation (in the notation of the coincidence site lattice) formed in a copper-bismuth alloy by the reversible faceting which

was induced by the segregation of bismuth.[17]

The computer modeling of atomic structures of grain boundaries has usually been made using empirical pair and, more recently, many-body (embedded atom type) interatomic potentials to describe the total energy of the system as a function of atomic positions.[18–20] These potentials are generally fitted to reproduce a variety of experimental data for the material studied. Exceptions are fully self-consistent *ab initio* calculations of the structure and energy of (001) twist boundaries in germanium,[21] tight-binding calculations of grain boundaries in silicon[22,23] and calculations utilizing first principles pair potentials, for example, the potential for aluminum derived on the basis of the pseudopotential theory.[15] Although calculations employing empirical potentials are most reliable when studying generic features common to whole classes of materials,[20,24] they have also been successful in revealing properties specific to certain materials, for example, surface reconstructions in noble metals.[25,26] Recently, quite reliable many-body potentials have also been constructed for binary alloys of noble metals[27] and for the nickel-aluminum alloys.[28,29] However, construction of empirical potentials for binary alloys is frequently hindered by insufficient experimental data needed for fitting of the potential parameters. This is particularly so when the system studied forms no ordered alloys or compounds and possesses a low solubility. This is the situation encountered in the case of the copper-bismuth alloy for which the only experimental data available is the enthalpy of mixing for the liquid copper-bismuth solution at 1200 K.[30]

In this paper we first present the construction of the many-body empirical potentials for copper-bismuth alloys. The proposition here is to use several quantities calculated using an *ab initio* method within the local-density approximation for a conjectural $L1_2$ Cu_3Bi compound when fitting the potentials. The validity of the constructed many-body potentials is then assessed by comparison with additional *ab initio* calculations. However, the most important demonstration of their applicability is provided by the analysis of the atomic structure of the above mentioned $\Sigma=3$ $(111)/(11\bar{1})$ grain boundary facet containing a high concentration of bismuth. The latter represents the second part of the paper which is devoted to the detailed structural examination of this boundary which combines HREM and computer modeling and leads to an excellent agreement between the experiment and the theory.

II. MANY-BODY POTENTIALS FOR COPPER-BISMUTH ALLOYS

The potentials describing atomic interactions were constructed employing the Finnis-Sinclair scheme[19] modified for alloys.[27,29] In this approach the total energy of the system of N atoms is written as

$$E=\sum_{i=1}^{N}\left[\frac{1}{2}\sum_{j\neq 1}V_{S_iS_j}(R_{ij})-\sqrt{\rho_{S_i}}\right], \tag{1a}$$

where

$$\rho_{S_i}=\sum_{j\neq i}\Phi_{S_iS_j}(R_{ij}) . \tag{1b}$$

Suffices i and j refer to individual atoms and the suffices S_i and S_j refer to the species of the atoms involved. Both V and Φ are empirically fitted pair potentials and summation over j extends over those neighbors of the atom i for which R_{ij} is within the cut-off radii of these potentials. The first term is a sum of pair-potential interactions and the second term the many-body attractive part of the cohesive energy. The square root dependence of the latter term is justified when developing this scheme from a tight-binding approach which incorporates orbital charge conservation at individual atoms and utilizes the approximation of the second moment of the density of states; the potentials Φ are then identified with the squares of the corresponding hopping integrals.[19,31]

For the binary systems the pair potentials constituting the semiempirical scheme proposed by Ackland and Vitek[27] are denoted V_{AA}, V_{BB}, V_{AB}, Φ_{AA}, Φ_{BB}, and Φ_{AB}. Functions V_{AA}, V_{BB}, Φ_{AA}, and Φ_{BB} were taken to be the same as those for pure elements. The function Φ_{AB} was chosen as a geometrical mean of Φ_{AA} and Φ_{BB} which is congruent with its interpretation in terms of hopping integrals. Hence, only the pair potential V_{AB} was fitted to alloy properties. However, in the present paper we not only fit the potential V_{CuBi} but also rescale the potentials V_{BiBi} and Φ_{BiBi} when fitting the alloy properties as described below.

In order to be consistent with the functional forms used for the pure elements,[32] we employed cubic splines for V_{AB} so that the functions which make up the present model are

$$\begin{aligned}
V_{AA}(R_{ij})&=\sum_{k=1}^{6}a_k^{AA}H(r_k^{AA}-R_{ij})(r_k^{AA}-R_{ij})^3 ,\\
\Phi_{AA}(R_{ij})&=\sum_{k=1}^{2}A_k^{AA}H(R_k^{AA}-R_{ij})(R_k^{AA}-R_{ij})^3 ,\\
V_{AB}(R_{ij})&=\sum_{k=1}^{3}a_k^{AB}H(r_k^{AB}-R_{ij})(r_k^{AB}-R_{ij})^3 ,
\end{aligned} \tag{2}$$

where $H(x)$ is the Heaviside step function. V_{BB} and Φ_{BB} have, of course, the same form as V_{AA} and Φ_{AA}. For copper and bismuth the parameters a_k^{AA}, A_k^{AA}, r_k^{AA}, and R_k^{AA} are summarized in Table I and parameters a_k^{CuBi} and r_k^{CuBi} are presented in Table II. The fitting procedure through which these potential parameters were determined is discussed below.

The many-body potentials can conveniently be visualized using the effective pair potentials.[19] The original definition was for pure elements but generalization to binary alloys is straightforward and the effective pair potentials for species S_1 and S_2 can be written as

$$V_{S_1S_2}^{\mathrm{eff}}(R)=V_{S_iS_2}(R)-\left[\left[\frac{c_{S_1}}{\sqrt{\rho_{S_1}^0}}+\frac{c_{S_1}}{\sqrt{\rho_{S_2}^0}}\right]\right]\Phi_{S_1S_2}(R) \tag{3}$$

where c_{S_1} and c_{S_2} are concentrations of species S_1 and

TABLE I. Potential parameters for V_{AA} and Φ_{AA} for copper and bismuth; a_k and A_k are in eV and r_k and R_k in units of the lattice parameter a. $a=3.615$ Å for copper, $a=3.800$ Å for pure bismuth in the bcc form and $a=3.565$ Å for the scaled Bi-Bi potentials used in Cu-Bi alloys.

	Copper	Bismuth		Copper	Bismuth
a_1	61.735 259	0.000 000	r_1	1.225	1.250
a_2	−108.184 679	−58.981 927	r_2	1.202	1.200
a_3	57.000 539	125.198 490	r_3	1.154	1.150
a_4	−12.887 966	−94.793 563	r_4	1.050	1.050
a_5	39.163 819	96.254 010	r_5	0.866	0.900
a_6	0.000 000	30.792 014	r_6	0.707	0.866
A_1	10.037 183	7.512 826	R_1	1.225	1.250
A_2	17.063 633	−9.795 798	R_2	0.990	1.050

S_2, respectively, and $\rho^0_{S_1}$ and $\rho^0_{S_2}$ are evaluated for a reference structure. The physical meaning of this potential is that it describes the atomic interactions when the second and higher derivatives of the many-body attractive part can be neglected. The latter assumption applies if the density of the structure studied does not differ appreciably from the density of the reference structure. In the following we use the effective pair potentials to display the constructed many-body potentials.

A. Potentials for pure copper

The detailed explanation of the method of construction of Finnis-Sinclair potentials for pure elements can be found in Refs. 19 and 32. The potentials for copper used in the present study are very similar to those developed in Ref. 32 but they have been modified so as to eliminate the "bump" in the pair potential, V_{CuCu}, between second and third neighbors.[27,29] Both V_{CuCu} and Φ_{CuCu} are cut off at the third nearest-neighbor separation and the pair potential V_{CuCu}, is purely repulsive. These potentials reproduce the equilibrium lattice parameter a, cohesive energy, E_c, elastic moduli C_{11}, C_{12}, and C_{44}, the vacancy formation energy, E_v^f, and the $1/6\langle 112\rangle/(111)$ stacking fault energy, γ. All these quantities are summarized in Table III. The effective pair potential, $V^{\mathrm{eff}}_{\mathrm{CuCu}}$, for which the reference structure is the ideal fcc lattice is shown in Fig. 1.

B. Potentials for pure bismuth

At room temperature and atmospheric pressure bismuth crystallizes in a body-centered trigonal structure with a trigonal angle of 57°.[33] This phase is semimetallic and so the essential assumption for the construction of the many-body potentials defined by Eqs. (1a) and (1b), charge conservation at individual atoms, may not be valid.[31] However, we are not interested in using this potential for studies of pure bismuth but for defect calculations in copper-bismuth alloys at bismuth concentrations well below 50%. In these alloys bismuth is effectively subject to a very high pressure owing to much smaller volume per atom in copper than in bismuth. At the pressure of 90 kbar the trigonal bismuth transforms into a metallic body-centered-cubic structure.[34] Hence, many-body potentials of the type used here are a valid approximation for the description of atomic interactions in this high pressure form of bismuth. However, the only directly measured quantity for bcc bismuth is the lattice parameter[34] while the cohesive energy and elastic constants have only been measured for the trigonal phase.[33,35] We estimated, therefore, the cohesive energy and elastic moduli of the cubic phase on the basis of the corresponding quantities of the trigonal phase.

For materials which may possess different structures at different pressures the transition pressure can be determined from the common tangent of the dependences of the cohesive energy on volume for the alternative structures (see, for example, Ref. 36). In order to estimate the cohesive energy for bcc bismuth we inverted this procedure. Experimental values of the lattice parameters are known for both the trigonal and bcc high pressure phase of bismuth; they are 4.749 Å and 3.8 Å, respectively. The cohesive energy of the trigonal bismuth is $E_c^t=2.173$ eV and the pressure at which the transformation occurs, identified with the slope of the common tangent, is $p=90$ kbar. Following the common tangent construction the cohesive energy of the bcc phase may be estimated as $E_c=E_c^t-p(V_t-V_{\mathrm{bcc}})$, where V_t and V_{bcc} are volumes

TABLE II. Potential parameters for V_{CuBi}; a_k are in eV/Å^3 and r_k in Å.

a_1	−0.046 488	r_1	4.800
a_2	0.375 487	r_2	3.920
a_3	5.748 289	r_3	2.800

TABLE III. The quantities fitted by potentials for pure copper and bcc bismuth.

	Copper	Bismuth
E_c (eV)	3.518	1.75
a (Å)	3.615	3.800
C_{11} (eV/Å^3)	1.684	0.390
C_{12} (eV/Å^3)	1.214	0.132
C_{44} (eV/Å^3)	0.754	0.064
E_v^f (eV)	1.17	0.7
γ (mJm^{-2})	30−50	

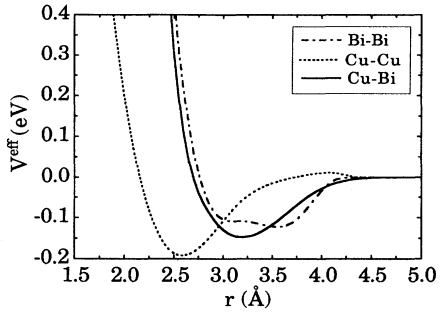

FIG. 1. Effective pair potentials for the copper-bismuth system.

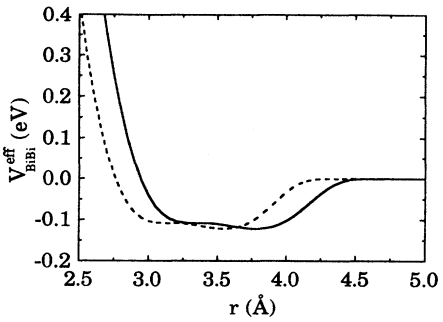

FIG. 2. Effective pair potentials for bismuth. The solid curve corresponds to the original potentials for bcc bismuth and the dashed curve to the scaled potential used in the case of the copper-bismuth alloys.

per atom in the trigonal and bcc phase, respectively. The calculated value of E_c which has been used when fitting the potentials for bismuth, is presented in Table III. A small error arises from the fact that the common tangent does not pass through the minima of the cohesive energy vs volume curves but in the present case this error is smaller than the uncertainties in the experimental values of E_c^t and p.

There is no analogous procedure which could be employed to determine with some confidence the elastic moduli of the bcc phase on the basis of those for the trigonal phase. However, in the body-centered-trigonal bismuth the trigonal angle is 57° and if it were 60° the structure would be simple cubic. This suggests that the deviation from the cubic symmetry is only small. Indeed, when choosing the coordinate system such that its axes are parallel to the edges of the cube which would result if the trigonal angle were 60°, the tensor of elastic moduli is very similar to that of a cubic crystal in the sense that those elastic moduli which are exactly zero in the cubic case, are much smaller than those which are nonzero for the cubic symmetry. Owing to the lack of other guidelines, we identified the elastic moduli of bcc bismuth with the moduli C_{11}, C_{12}, and C_{44} of the trigonal bismuth in this coordinate system; they are summarized in Table III.

Finally, the vacancy formation energy was used as a fitting parameter when constructing the many-body potentials for pure metals. In the case of bismuth this has not been measured for either trigonal or bcc structure. However, in many metallic systems the vacancy formation energy is close to one third of the cohesive energy and thus we took $E_v^f = E_c/3$; this is the value given in Table III. The fitting of the potentials V_{BiBi}, and Φ_{BiBi}, which are cut-off between the second and third nearest-neighbor separation, was then performed in the same way as in the case of Cu and other pure elements.[32] The effective pair potential V^{eff}_{BiBi}, for which the reference structure is the bcc lattice of bismuth, is shown in Fig. 2 by the solid curve. Using this potential we calculated the cohesive energies of the following structures: fcc, hcp with the ideal c/a ratio, simple cubic, simple hexagonal, diamond, graphite, and A15 lattice. In each case the corresponding lattice parameter was found by minimizing the energy at the external pressure of 90 kbar. For all these structures the cohesive energy was found to be lower than for the bcc phase and thus the constructed potential, indeed, prefers the bcc structure over a number of other alternatives.

C. Potentials for alloys

Since copper and bismuth do not form any ordered structures and the solubility of bismuth in copper is very low [about 0.003 at. % at 800 °C (Ref. 37)], there are virtually no experimental data to be fitted for the copper-bismuth system. Attempts to construct potentials for this system have been made in the past but met only with a limited success. For example, Maeda, Vitek, and Sutton[38] took the measured enthalpy of mixing in the liquid solution[30] to be the same in the solid solution and assumed that the average atomic volume follows Vegard's law. In order to obtain more reliable fitting parameters we calculated the total energy of a metastable $L1_2$, fcc based, Cu_3Bi compound as a function of the volume per atom and as a function of the applied tetragonal and trigonal shear strains. These calculations, described in more detail in Appendix A, were performed using the all-electron self-consistent full-potential linear-muffin-tin-orbital method within the local-density approximation.[39,40] As a result we obtained the equilibrium lattice parameter, the bulk modulus, the tetragonal shear modulus $G=\frac{1}{2}(C_{11}-C_{12})$ and the trigonal shear modulus C_{44} for this metastable compound. These calculated quantities, which are summarized in Table IV, were then used as "empirical" data.

In the present scheme the equilibrium condition $dE/d\Omega=0$, where Ω is the volume of the unit cell, leads to the equation

$$\sum_{i=1}^{4}\sum_{j\neq i}\left[V'_{S_iS_j}(R_{ij})-\frac{1}{\sqrt{\rho_{S_i}}}\Phi'_{S_iS_j}(R_{ij})\right]R_{ij}=0\ , \tag{4}$$

where the summation over i includes four atoms of the unit cell of the $L1_2$ structure and the summation over j extends over all the neighbors interacting with the atom i. The bulk modulus $B=-\Omega(d^2E/d\Omega^2)$ is then

TABLE IV. The lattice parameter, a, bulk modulus, B, and shear moduli, G and C_{44}, calculated for metastable Cu_3Bi and CuBi compounds using the *ab initio* method and constructed many-body potentials, respectively.

	Cu_3Bi in the $L1_2$ structure		CuBi in the B2 structure	
	Ab initio calculation	Present potentials	*Ab initio* calculation	Present potentials
a (Å)	3.909	3.909	3.410	3.440
B (eV/Å^3)	0.743	0.743	0.619	0.368
G (eV/Å^3)	0.144	0.144	0.115	−0.050
C_{44} (eV/Å^3)	0.324	0.442	0.125	0.252

$$B=\frac{1}{72\Omega}\sum_{i=1}^{4}\left\{\sum_{j\neq i}\left[V''_{S_iS_j}(R_{ij})-\frac{1}{R_{ij}}V'_{S_iS_j}(R_{ij})-\frac{1}{\sqrt{\rho_{S_i}}}\left[\Phi''_{S_iS_j}(R_{ij})-\frac{1}{R_{ij}}\Phi'_{S_iS_j}(R_{ij})\right]\right]R_{ij}^2+\frac{1}{2\sqrt{\rho_{S_i}^3}}\left[\sum_{j\neq i}\Phi'_{S_iS_j}(R_{ij})R_{ij}\right]^2\right\} \tag{5}$$

and the tetragonal and trigonal shear moduli are

$$G=\frac{1}{16\Omega}\sum_{i=1}^{4}\left\{\sum_{j\neq i}\left[V''_{S_iS_j}(R_{ij})-\frac{1}{R_{ij}}V'_{S_iS_j}(R_{ij})-\frac{1}{\sqrt{\rho_{S_i}}}\left[\Phi''_{S_iS_j}(R_{ij})-\frac{1}{R_{ij}}\Phi'_{S_iS_j}(R_{ij})\right]\right]\times\frac{X_{ij}^2(X_{ij}^2-Y_{ij}^2)}{R_{ij}^2}+\frac{1}{2\sqrt{\rho_{S_i}^3}}\left[\sum_{j\neq i}\Phi'_{S_iS_j}(R_{ij})\frac{X_{ij}^2}{R_{ij}}\right]\left[\sum_{k\neq i}\Phi'_{S_iS_k}(R_{ik})\frac{X_{ik}^2-Y_{ik}^2}{R_{ik}}\right]\right\} \tag{6}$$

and

$$C_{44}=\frac{1}{8\Omega}\sum_{i=1}^{4}\left\{\sum_{j\neq i}\left[V''_{S_iS_j}(R_{ij})-\frac{1}{R_{ij}}V'_{S_iS_j}(R_{ij})-\frac{1}{\sqrt{\rho_{S_i}}}\left[\Phi''_{S_iS_j}(R_{ij})-\frac{1}{R_{ij}}\Phi'_{S_iS_j}(R_{ij})\right]\right]\times\frac{X_{ij}^2Y_{ij}^2}{R_{ij}^2}+\frac{1}{2\sqrt{\rho_{S_i}^3}}\left[\sum_{j\neq i}\Phi'_{S_iS_j}(R_{ij})\frac{X_{ij}Y_{ij}}{R_{ij}}\right]^2\right\} \tag{7}$$

where X_{ij} and Y_{ij} are x and y components of the vector connecting atoms i and j in the cube coordinate system.

The fitting of the potential parameters then proceeded as follows. As explained above, in the present scheme

$$\Phi_{CuBi}(R_{ij})=\sqrt{\Phi_{CuCu}(R_{ij})\Phi_{BiBi}(R_{ij})}\ . \tag{8}$$

In the first approximation the Cu-Cu and Bi-Bi potentials were taken as those constructed for pure elements and thus at this stage only the parameters of the potential V_{CuBi} were determined so as to fit the data for the alloy. The cut-off radius, r_1^{CuBi}, was fixed at a value between the third and fourth nearest-neighbor separation in the copper lattice so that the ranges of Cu-Cu and Cu-Bi interactions are similar. Two of the coefficients a_k^{CuBi} for the potential V_{CuBi} were then determined for chosen values of r_k^{CuBi} such that Eqs. (4) and (5) were satisfied precisely, fitting thus exactly the lattice parameter and the bulk modulus of the theoretical Cu_3Bi compound. The third coefficient could be determined by fitting the cohesive energy of this compound using Eq. (1a). However, while the cohesive energy is also determined in *ab initio* calculations, its absolute value is notoriously imprecise in the framework of the local-density approximation and, therefore, it was not utilized in the fitting procedure. Instead, this coefficient was determined so as to reproduce the enthalpy of mixing for the liquid copper-bismuth solution at 1200 K, which was measured by Lomov and Krestovnikov,[30] as precisely as possible. The latter part of the fitting utilized a Monte Carlo simulation

which is described in more detail in Appendix B.

In the second step new values of the parameters r_k^{CuBi} were chosen and the Bi-Bi potentials scaled such that the equilibrium lattice parameter of the bcc bismuth is smaller than originally. This scaling corresponds to rigidly shifting the potentials V_{BiBi}, and Φ_{BiBi}, towards smaller values of r, as demonstrated in Fig. 2 by the scaled effective pair potential V_{BiBi}^{eff} (dashed curve). Physically, the scaling leads to a reduction of the size of the bismuth atoms which will be smaller when embedded in copper than in the pure form. The Cu-Cu potentials were not changed. This fitting procedure was then repeated for several different values of the parameters r_k^{CuBi} and several different scalings of the bismuth potentials, until the best fit was attained not only for the enthalpy of mixing but also for the shear moduli G and C_{44}. The Bi-Bi potentials used in the semiempirical scheme for Cu-Bi alloys are then the scaled potentials for which the best fit was achieved; they correspond to the lattice parameter of bcc bismuth $a_{Bi}=3.565$ Å. The corresponding effective pair potentials V_{CuBi}^{eff} (the reference structure the ideal $L1_2$ Cu_3Bi structure) and V_{BiBi}^{eff} for the scaled potentials (the reference structure the bcc lattice) are shown in Fig. 1.

A test of the constructed many-body potentials was performed by comparing the equilibrium lattice parameter and bulk and shear moduli of CuBi in the metastable B2, bcc based, structure, calculated using the potentials, with those evaluated *ab initio,* employing the same method as for the $L1_2$ Cu_3Bi. The latter calculations are again described in more detail in Appendix A. In the case of the B2 structure the equilibrium condition and the bulk and shear moduli are again given by Eqs. (5)–(7) but the summation over i extends now over two atoms of the unit cell of this structure. The results of both *ab initio* and many-body potential calculations are summarized in Table IV. It is seen that the lattice parameter of the B2 phase evaluated *ab initio* is well approximated by that calculated using the many-body potentials. Thus the volume per atom is well reproduced even for this high concentration of bismuth. However, the bulk and trigonal shear moduli are reproduced only within a factor of 2 and the tetragonal shear modulus is negative for the case of the many-body potentials, indicating that the B2 structure is in this scheme unstable with respect to the tetragonal shear deformation. Nonetheless, considering the very low solubility of bismuth in copper, concentration of bismuth as high as that encountered in the case of the B2 alloy is unlikely to be found either in the bulk or in the vicinity of extended defects such as interfaces. Hence, the constructed potentials are suitable for atomistic studies of extended defects in copper-bismuth alloys provided the concentration of bismuth is well below 50% although it can be close to or in excess of 25%. However, the ultimate test of the potentials is a comparison of calculated and observed structures; one such study combining calculations and HREM is presented in the following section.

III. ATOMIC STRUCTURE OF THE $\Sigma=3(111)(11\bar{1})$ TILT BOUNDARY

As mentioned in the Introduction, segregation-induced faceting of grain boundaries is a common phenomenon in copper-bismuth alloys.[7,9,10] This process is reversible in that the loss of bismuth from the boundaries results in a defaceting reaction.[8] In pure copper the $\Sigma=3(111)/(11\bar{1})$ symmetrical tilt boundaries with the rotation axis $[1\bar{1}0]$ and misorientation 70.53° are the coherent twin boundaries. Upon first examination, it does not seem likely that bismuth should segregate to these interfaces. Indeed, previous HREM results show that no segregation takes place to coherent twins if they are present in the sample prior to segregation.[14]

On the other hand, it was observed that in Cu-Bi alloys segregation of bismuth induces the formation of $(111)/(11\bar{1})$ facets which contain a high concentration of bismuth.[9,10] Considering that no direct segregation to the coherent twin takes place, these observations suggest that the $(111)/(11\bar{1})$ facets are formed by the transformation of other boundaries which already contain bismuth, in particular general curved boundaries with the $\Sigma=3$ misorientation. This conclusion agrees with a recent conventional TEM study[41] of grain boundary transformations in this system. In this work it was found that the initially curved grain boundaries faceted only after significant aging time and the faceted boundaries between grains with misorientation $\Sigma=3$ contained a high percentage of $(111)/(11\bar{1})$ facets.

The above experimental evidence indicates that segregation-induced faceting in the Cu-Bi system is associated with the formation of a new two-dimensional phase. Hence, the structure of these facets is of principal interest when studying the segregation-induced transformations of boundary structures and related effects on properties such as interfacial cohesion. Fortunately, the $(111)/(11\bar{1})$ facets are ideally suited for HREM analysis since the boundary plane does not deviate from the $\{111\}$ plane and it can thus be maintained parallel to the electron beam. This provides an excellent opportunity to carry out a combined experimental and theoretical investigation of their structures and assess at the same time the validity of the many-body potentials constructed in this paper. The main results of this study have been reported briefly in Ref. 17 and in this paper we present a more detailed analysis.

A. Model structure deduced from the HREM study

The HREM analysis has been performed using a JEOL JEM 4000EX microscope. The sample containing the above mentioned boundary was tilted such that the electron beam was aligned along the common crystal direction for both grains which is the rotation axis $[1\bar{1}0]$. Images were then recorded at several values of objective lens defocus. From the systematic variation of the image contrast with defocus we can extract information on both the positions and identities of the atoms.[13,14] In general, this involves an iterative process in which calculated images of model structures are compared to the experimental images. When interpreting these images, many model structures, commensurate with the observed periodicities within the interface, were first constructed geometrically, without any consideration of the energy and stability of these structures. Comparison with the experiment was then made by calculating images arising from these mod-

els as a function of defocus using the multislice formalism.[42] Material and microscope parameters of the calculation were determined using the images of the bulk copper grain away from the boundary for calibration. In this way, the specimen thickness, microscope focal spread and beam convergence as well as the defocus corresponding to each image, were determined.

The model structure which led to the best match of calculated and observed images can be described as follows.[43] In the framework of the "ABC" depiction of the sequence of $\{111\}$ atomic planes in an fcc crystal, the $\Sigma=3(111)/(11\bar{1})$ twin in pure copper can be represented as

$$A\text{-}B\text{-}C\text{-}A\text{-}B\text{-}\underset{|}{C}\text{-}B\text{-}A\text{-}C\text{-}B\text{-}A\text{-}C\ , \tag{9}$$

where the vertical lines mark the position of the boundary. The reconstructed model structure could be represented in the same way but in the marked layer C of (9) one third of the copper atoms are replaced by hexagonally arranged Bi atoms. However, the Bi atoms are centered outside this atomic plane so that a physically more appropriate representation of the model structure is

$$A\text{-}B\text{-}C\text{-}A\text{-}B\text{-}C'\underset{|}{|}C(\mathrm{Bi})\text{-}B\text{-}A\text{-}C\text{-}B\text{-}A\ , \tag{10}$$

where C' denotes a plane of copper atoms in which one third of the atoms were replaced by hexagonally arranged vacancies, and C(Bi) the plane of bismuth atoms positioned above these vacancies.

B. Simulated structure

The atomistic modeling of the $\Sigma=3(111)/(11\bar{1})$ boundary in copper bismuth was carried out using the structure described by (10) as a starting configuration. The calculation was then carried out as follows. A block of (copper) atoms, containing the boundary studied was first constructed geometrically. The boundary region was then modified by replacing some of the copper atoms by bismuth atoms so as to form the structure described above. The relaxation calculation was then performed using a molecular statics technique in which the total energy of the block, given by Eq. (1a), has been minimized with respect to the positions of the individual atoms as well as with respect to the relative rigid body displacement of the two adjoining grains. This displacement has components both parallel and perpendicular to the boundary so that there are neither any tensile nor compressive stresses normal to the boundary nor shear stresses parallel to the boundary present in the final configuration. The displacement perpendicular to the boundary represents the expansion and thus the calculation corresponds to relaxation at constant pressure.

In the direction perpendicular to the boundary the block is effectively infinite but it was found that it was sufficient to limit the relaxation to twenty two $\{111\}$ layers on each side of the boundary. In the directions parallel to the boundary periodic boundary conditions have been maintained throughout the calculation. The smallest possible repeat cell of this structure is $\frac{3}{2}[1\bar{1}0]\times\frac{1}{2}[11\bar{2}]$. However, reconstructions leading to larger unit cells may occur, similarly to what has been observed in the case of free surfaces.[44] For this reason calculations were also carried out for larger repeat cells of the type $n\frac{3}{2}[1\bar{1}0]\times m\frac{1}{2}[11\bar{2}]$, where n and m are integers. However, the same structures were found for $n=m=1$, $n=1$, and $m=2$ as well as for $n=2$ and $m=4$.

The relaxed structure is shown in Fig. 3 where copper atoms are represented by small circles and the bismuth atoms by large circles and also distinguished by shading. In Fig. 3(a) the structure is projected onto the $(1\bar{1}0)$ plane and no distinction is made between atoms belonging to the six subsequent $(1\bar{1}0)$ planes which comprise one repeat distance of the unit cell in the $[1\bar{1}0]$ direction. In Fig. 3(b) the structure is projected onto the (111) plane. For reasons of clarity only one (111) layer of copper atoms from the lower grain and the bismuth layer adja-

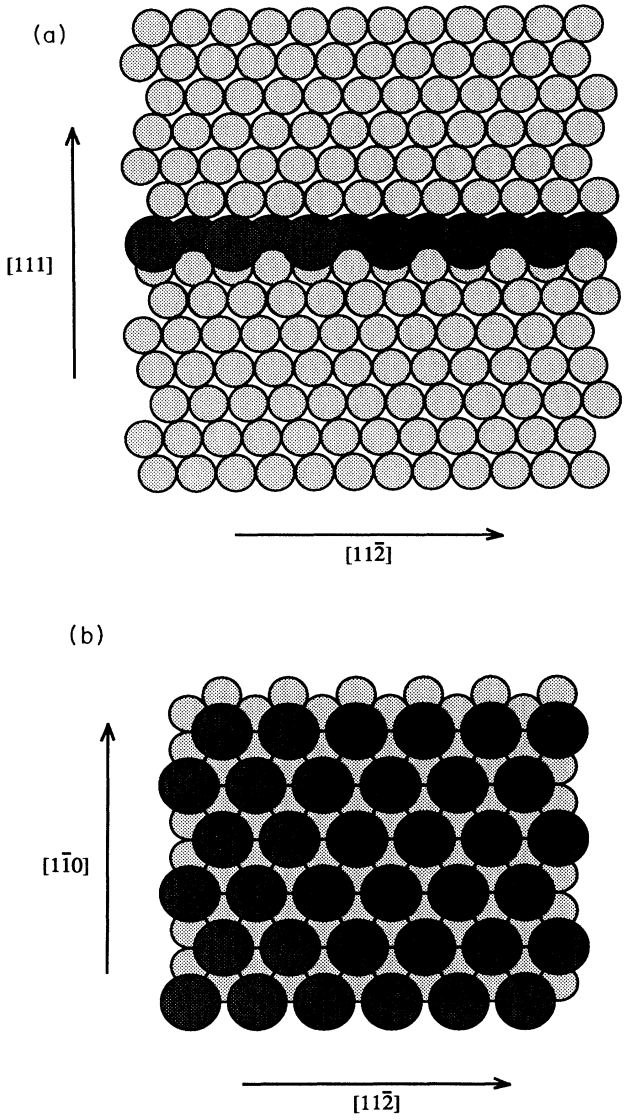

FIG. 3. The relaxed structure of the $\Sigma=3(111)/(11\bar{1})$ boundary containing bismuth. (a) The structure projected onto the $(1\bar{1}0)$ plane. (b) The structure projected onto the (111) plane.

cent to it are shown; no atoms belonging to the upper grain are displayed.

The overall expansion of the bi-crystal, caused by the rigid body displacement of the two grains across the boundary, is 1.88 Å. This is not far from one interplanar spacing of {111} planes in Cu (2.087 Å) and thus the boundary structure can be interpreted to a good approximation as splitting of one of the {111} planes, C, into two, C' and C(Bi) planes, containing Cu and Bi, respectively. The boundary is not, therefore, symmetric in the sense that there is no mirror symmetry across the geometrical boundary plane as it is in the twin boundary in a pure fcc material. Furthermore, the expansion is not concentrated only between the layers adjacent to the layer of bismuth but spreads nonuniformly across a number of {111} layers (≈ 8). In particular, the separation between the layer of bismuth atoms [C(Bi)] and the layer of copper atoms with vacancies (C') is 1.46 Å, while the separation between the next layer of copper atoms and the bismuth layer is 2.65 Å. Thus, while the bismuth atoms [i.e., the whole layer C(Bi)] are contracted towards the plane of copper containing vacancies (C'), the overall expansion between the copper layer C' and the copper layer above the bismuth layer is 2.023 Å and, therefore, a small overall contraction, 0.14 Å, must occur in between copper layers further away from the bismuth layer.

C. Comparison between simulated and observed structures

In order to make a detailed comparison of the calculated and observed structures, a series of images, corresponding to the same defocus conditions and thickness as in the HREM study, were calculated for the relaxed structure using the multislice formalism. The parameters for the multislice calculation are presented in Table V. The critical parameters of thickness and defocus were determined using the images of the copper grains adjacent to the boundary for calibration. For the alloy system studied, the assumption that the grains are pure copper is valid due to the low bulk solubility of bismuth in copper at 600 °C (Ref. 37) which was the aging temperature; at equilibrium, there should be one bismuth atom

TABLE V. Material and microscope parameters used in the image simulations.

Slice dimensions	
$[11\bar{2}]$	4.43 Å
[111]	42.67 Å
$[1\bar{1}0]$	1.28 Å
Maximum spatial frequency in reciprocal space	
$[11\bar{2}]$	4.82 $Å^{-1}$
[111]	8.00 $Å^{-1}$
Thickness	38.34 Å
Focal spread	100 Å FWHM
Convergence	2 mrad
C_s	1 mm
Defocus	−316 Å, −636 Å, −828 Å, −1020 Å

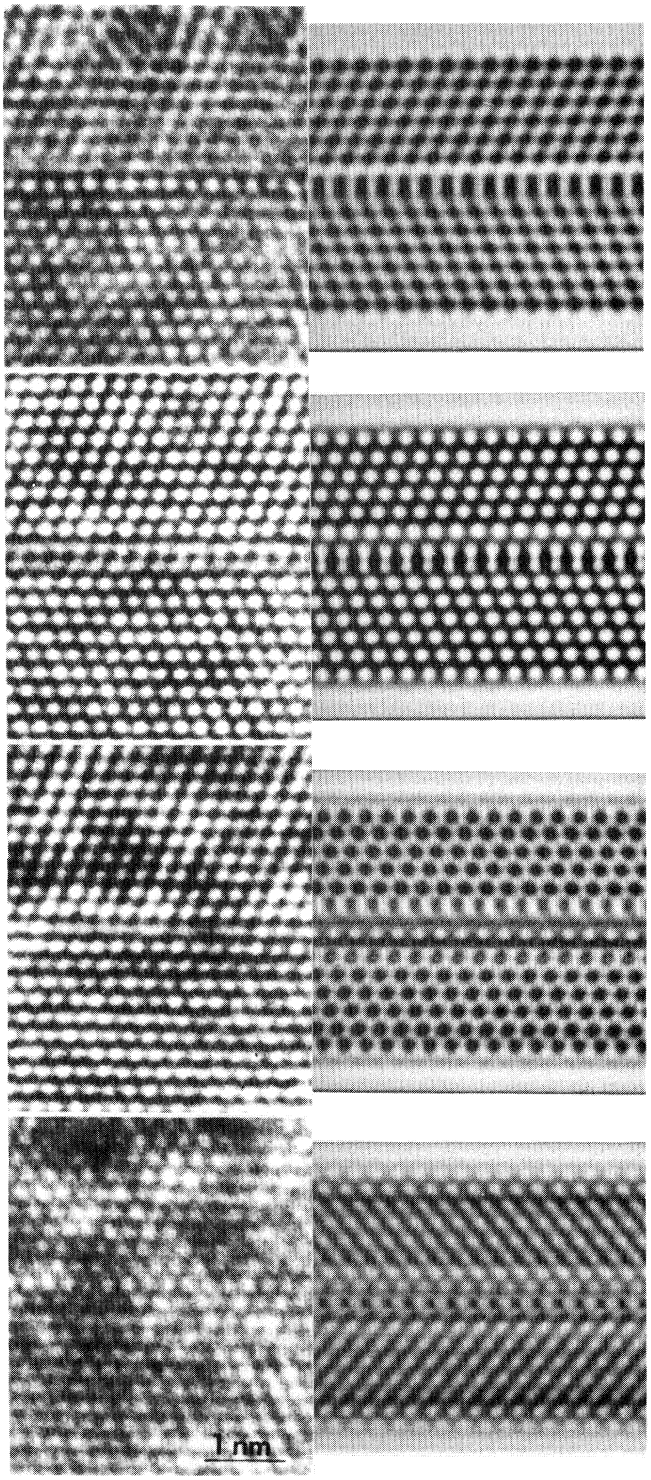

FIG. 4. Experimental (left column) and calculated (right column) image series with objective lens underfocus increasing down the figure. The marker represents 15 Å.

for every 2740 copper atoms.

The results of the image simulations are presented in Fig. 4. In this picture, increasing underfocus (-316 to -1020 Å) runs down the page; the images corresponding to the calculated structure are in the right column and the experimental images in the left column. The calculated images clearly reproduce the systematic contrast changes in the experimental image. Most importantly, the periodicities within the boundary plane along the $[11\bar{2}]$ direction are preserved as is the expansion of the structure in the [111] direction, perpendicular to the boundary plane. In the first image, the boundary consists of a centered row of discrete light contrast with a slight asymmetry of the contrast of the first pure Cu plane bounding the interface. In the second image, the boundary appears as a ladder structure with streaking present between the atom contrast within the interface. In the third image, the boundary again consists of light contrast centered in the boundary although it tends to be more diffuse than in the first image. In the fourth image, it is seen that the (200) fringes terminate adjacent to dark contrast in the boundary.

The degree of match in the image series is strong evidence for the very high accuracy with which the structure has been predicted theoretically. The contrast clearly reflects the asymmetric nature of the boundary structure described above. In the images of Fig. 4, the contrast above the boundary plane tends to be somewhat stronger than that below the plane. This contrast is a Fresnel effect arising from the asymmetrical position of the bismuth atom plane in the interface. Furthermore, the total calculated expansion (1.88 Å), i.e., the relative displacement of the two grains in the direction perpendicular to the boundary, is within the experimental limits of the accuracy in the HREM (≈ 0.1 Å), in a perfect agreement with the experiment.

IV. DISCUSSION

The results presented here demonstrate that HREM studies and theoretical structural analyses can be used synergistically to decipher with a great accuracy the structure of grain boundaries containing multiple atomic species. At the same time these results provide a firm evidence that the empirical central force many-body potentials are capable to describe with a sufficient accuracy atomic interactions even in relatively complex systems such as Cu-Bi provided an appropriate and sufficient input is used in their construction. For this purpose the use of self-consistent *ab initio* electronic structure calculations to provide "empirical" data was of principal significance since this allows sampling of crystal configurations which are not attainable experimentally. This approach was also employed very successfully when constructing potentials describing the interaction of boron with nickel and aluminum in the Ni_3Al compound.[45]

The *ab initio* calculations were performed using the all-electron self-consistent full-potential linear-muffin-tin-orbital method within the local-density approximation[39,40] and the data obtained are the equilibrium lattice parameter, the bulk modulus and the tetragonal and trigonal shear moduli for metastable Cu_3Bi in the $L1_2$ structure. While the moduli provide important information on the response of the structure to shear and dilatational strains, the most important information acquired is the equilibrium density of the Cu-Bi alloy at bismuth concentrations comparable to those found in the boundaries studied, i.e., the atomic size of bismuth in copper. As seen from Table IV, the calculated volume per atom in Cu_3Bi is 26% larger than in pure copper and in CuBi 68% larger. If the Vegard's law is applied then the volume per atom would be 33% and 66% larger than in pure copper for Cu_3Bi and CuBi, respectively, when using the bcc bismuth as the reference state. Although the deviation of the calculated atomic volumes from the Vegard's law is not very large, if used as a guideline for fitting the potentials the size of the bismuth atom in copper would be appreciably overestimated at lower concentrations of bismuth. At the same time when studying segregation and interfacial structures the size effect is a very important and, possibly, governing parameter. Hence, the correct estimation of this parameter is the most significant contribution of the *ab initio* total energy calculations performed in this study. Comparison of calculations employing the constructed potentials with additional *ab initio* calculations for a metastable B2 CuBi alloy shows that these potentials can be employed for a wide range of bismuth concentrations when considering the size effect, although shear instabilities might arise at high bismuth concentrations.

However, the most important test of the applicability of the constructed potentials is the comparison between the calculated structure of the $\Sigma=3(111)/(11\bar{1})$ grain boundary containing bismuth and the HREM observations. The overall quality of the match between experimental images and images calculated for the relaxed structure of this boundary is quite remarkable. The series of images produced via simulation reproduces all the important features of the experimental images including the periodicities of the boundary structure, the relative rigid-body displacements of the adjoining grains across the interfaces, in particular the expansion across the boundary, the systematic changes in contrast with increasing defocus, the termination of lattice fringes at the interface and even the special Fresnel effects due to the asymmetrical position of the bismuth atoms within the interface. There are two features, best seen by comparing the second images in the series (defocus $=-636$ Å), which are less pronounced in the simulated images than in the experimental images.

Firstly, in the second image the contrast in the interface is composed of white dots which are interconnected by diffuse streaks. These streaks are stronger in the experimental image than in the simulated image. The most likely origin of this discrepancy is that the model of the interface is an ideal periodic boundary in an infinite bicrystal while in reality the boundary contains defects or distortions within the material or due to the intersection of the interface with the crystal surface. Since each image is a two-dimensional projection of a three-dimensional structure, any deviations from the model structure will be integrated through the thickness. The presence of these defects or distortions could lead to a

smearing of contrast in the images at certain defocus values; in fact, it is at this value of objective lens defocus that the HREM can most sensitively detect local displacements of atoms. [It is important to point out the variation in the sensitivity of the images to different features of the structure at different values of the objective lens defocus. We have found that images at defocus values near the value for the second image are most sensitive to changes in atom position in which the atoms do not move as a rigid close-packed plane. This is most likely due to the greater degree to which the displacement of individual atoms or columns of atoms are reproduced in the HREM image; this effect has been referred to as localization[46] and has been shown to be maximized at defocus values in this range for nominal atom separations in the range of 2 Å.[47] In contrast, images at this defocus value are not sensitive to rigid shifts in lattice planes, for example, the contraction of the bismuth atomic plane (C_{Bi}) into the adjacent copper plane containing vacancies (C'). In this case, a greater sensitivity for this structural feature is seen at defocus values lower and higher than that of the second image. Therefore, especially for the case of alloys, cursory observation of a single image or even a calculated match to a single experimental image will not be sufficient to study complex boundary structures especially when those boundaries contain multiple atomic species.]

A second aspect of the second experimental image, which is not fully reproduced in the model calculations, is that the pairs of white dots within the interface, i.e., C' and C(Bi) layers, nominally positioned such that the line connecting them is perpendicular to the interface plane, are slightly rotated out of this perpendicular alignment; e.g., the image of the C(Bi) layer is slightly shifted along the $[11\bar{2}]$ direction away from the C position. This feature cannot be reproduced by varying the image simulation parameters within the boundary conditions of the current experiments. A possible origin of this misaligned contrast was discussed previously by Luzzi.[14] If some bismuth has been lost from the material near the surface, the interface would be capped by the ideal $(111)/(11\bar{1})$ twin structure near the surfaces. This sandwich consisting of ideal twin/interface with Bi/ideal twin would then be viewed in projection ($[1\bar{1}0]$) in the HREM. With the constraint that the material away from the interface must be good bulk copper, the structure would be as follows:

Twin near surface: $A\text{-}B\text{-}C\text{-}A\text{-}B\text{-}C\text{—}A\text{—}B\text{-}A\text{-}C\text{-}B\text{-}A\text{-}C\text{-}B\text{-}A,$
Interior: $A\text{-}B\text{-}C\text{-}A\text{-}B\text{-}C'\text{-}C(\mathrm{Bi})\text{-}B\text{-}A\text{-}C\text{-}B\text{-}A\text{-}C\text{-}B\text{-}A,$
Twin near surface: $A\text{-}B\text{-}C\text{-}A\text{-}B\text{-}C\text{—}A\text{—}B\text{-}A\text{-}C\text{-}B\text{-}A\text{-}C\text{-}B\text{-}A,$

As imaged by the HREM (in $[1\bar{1}0]$ projection), the three structures are in perfect registry on both sides of the interface. Within the interface, the C' defective copper layer remains in registry with the surface twins, e.g., C above C' above C. However, the C(Bi) layer is now out of phase with the twinned layers, e.g., A above C(Bi) above A. When viewed in projection along $[1\bar{1}0]$ direction, the atoms in these A and C layers are displaced with respect to each other by $a/12[11\bar{2}]$. Since magnitude of this displacement is well beyond the resolution capabilities of the HREM, the projected image of the atoms will be shifted to a position intermediate between the A and C positions. This produces an apparent rotation of the pair of white dots [C' and C(Bi)] as seen in the image. It can also be expected that loss of bismuth near the surface would lead to structural relaxations at the boundary between the interior and surface layers. These relaxations could lead to the diffuse imaging effects discussed above which are seen in the image at this value of defocus.

In spite of the two features of the images discussed above, the overall quality of the match between experimental images and calculated images of the theoretically determined relaxed structure of the $\Sigma=3(111)/(11\bar{1})$ facet containing bismuth, is quite remarkable. This agreement represents an excellent validation for the constructed many-body potentials for the copper-bismuth system which can now be used with a high confidence to investigate the structure of those grain boundaries which are experimentally inaccessible as well as related atomic level processes such as kinetics of segregation and associated structural transformations in the boundaries.

ACKNOWLEDGMENTS

The authors are grateful for the use of the University of Pennsylvania MRL central facilities and would like to thank D. A. Ricketts-Foot for maintaining the microscope and Dr. B. Blum for preparing the specimens. This research was supported by the National Science Foundation, MRL Program DMR88-19885 (D.E.L.) and by the U.S. Department of Energy, Office of Basic Energy Sciences, Grant No. DE-FG02-87ER45295 (M.Y., M.S., V.V., G.J.A.). The computations were performed at the computing facility of the Laboratory for Research on the Structure of Matter supported by the National Science Foundation, MRL Program DMR88-19885 and at the Pittsburgh Supercomputing Center.

APPENDIX A: METHOD OF CALCULATION OF THE TOTAL ENERGY AND ELASTIC MODULI

The all-electron self-consistent full-potential linear-muffin-tin orbital (FP-LMTO) method developed within the local-density approximation[39,40] was used to calculate the equilibrium lattice parameters, the bulk moduli, the tetragonal shear moduli, $G=\frac{1}{2}(C_{11}-C_{12})$ and the trigonal shear moduli, C_{44}, for metastable Cu_3Bi in the $L1_2$ structure and CuBi in the B2 structure. In these calculations the total energy of the system was first evaluated as a function of the lattice parameter and the equilibrium lattice parameter ascertained from the minimum of the energy. The bulk modulus was then found from the second derivative of the total energy with respect to the

lattice parameter. Similarly, to evaluate the shear moduli the total energy was calculated as a function of the corresponding shear distortion and the second derivative determined the corresponding shear modulus. The second derivatives of the total energy were evaluated by numerical differentiation. Both structures studied are stable with respect to tetragonal and trigonal distortions. However, their total energy is higher than the weighted sum of the total energies of pure components, so that their formation is not energetically favorable and they are, therefore, metastable structures.

In the FP-LMTO method no assumptions are made about the potential or charge density and the muffin-tin geometry is employed only when constructing the basis functions, the muffin-tin orbitals (MTO's). For this purpose the space is divided into nonoverlapping muffin-tin (MT) spheres and the interstitial region. The MTO's are then constructed following the scheme proposed by Andersen, Jepsen, and Glötzel.[48] The total energy functional is evaluated for the full charge density and no spheroidization is introduced. In order to represent properly the charge density in the interstitial region, the basis set has to involve more MTO's than in the standard LMTO calculations employing the atomic sphere approximation where only MTO's with zero kinetic energy ($\kappa^2=0$) are retained.[48,49] The additional MTO's correspond to negative kinetic energies ($\kappa^2<0$) and the so called triple-κ basis set which includes $\kappa^2=0$ and two negative values of κ^2, is usually utilized. The FP-LMTO method employed in this study comprises an effective numerical treatment of three-center integrals which are reduced to a linear combination of two-center integrals.[39] The charge density in the interstitial region is represented by a linear combination of Hankel functions and the Poisson equation is solved analytically in the interstitial region; inside the MT sphere it is solved by a straightforward numerical integration. Thus the calculations are much faster than in many other full-potential treatments. This method has recently been applied very successfully in a variety of studies (for example, Ref. 50).

In the present calculations we used as the basis twenty two MTO's per atom which contain triple-κ s and p orbitals and double-κ d orbitals. The kinetic energies, κ^2, associated with the envelope Hankel functions are not critical and were taken here as 0.0, -1.0, and -3.0 Ry, respectively. The muffin-tin radii were always chosen to be 1.5% smaller than the radii of touching spheres in order to prevent overlapping of the spheres when applying shear strains. In the construction of the MTO basis the ratio of the muffin-tin radii for copper and bismuth, respectively, was identified with the ratio of the corresponding atomic radii (1.45). The core-electron charge density was not frozen but recalculated self-consistently in each iteration.

APPENDIX B: MONTE CARLO EVALUATION OF THE ENTHALPY OF MIXING

The definition of the enthalpy of mixing of a random A-B alloy is

$$\Delta H^{\text{mix}}=E^{\text{rand}}-c_A E^A-c_B E^B , \tag{B1}$$

where E^A and E^B are the cohesive energies of elements A and B in their pure states, respectively, c_A and c_B are their atomic fractions in the solution and E^{rand} is the cohesive energy of the solution. Since the experimental value of the enthalpy of mixing is known for the liquid at 1200 K the cohesive energies of copper and bismuth, entering Eq. (B1), have to correspond to this temperature. In the case of bismuth the cohesive energy at room temperature is 2.15 eV/atom.[51] The change of this energy with temperature was measured and at 1200 K it decreases by 0.38 eV/atom.[30] Hence, we take $E^{\text{Bi}}=1.77$ eV/atom (the experimental error is $\pm 19\%$). E^{Cu} is then taken as the cohesive energy of the supercooled copper liquid at 1200 K. This energy as well as E^{rand} have been obtained using the following Monte Carlo (MC) simulation procedure.

The simulation has been conducted at constant temperature, pressure, and total number of atoms. Periodic boundary conditions have been applied in all three directions and the repeat cell has been taken as a cube containing about two thousand atoms. Two types of variations of the simulated systems are considered in individual MC steps. The first corresponds to the displacement and/or interchange of atoms and the second to changing the total volume of the system which simulates the thermal expansion. In the single element system the first type of change is attained by randomly picking an atom in each MC step and displacing it by a small random amount. In the alloy two atoms are randomly chosen in each MC step and are allowed to exchange and randomly displace. The second type of change allows a small random change of the volume of the system studied. The decision whether to accept a given MC step is then made according to the probability

$$P=\left[1+\frac{\Delta V}{V}\right]^N \exp(-\Delta E/kT) , \tag{B2}$$

where ΔE is the energy change associated with the new configuration, ΔV is the change of the total volume of the system and V its original volume, N is the total number of atoms in the system, k the Boltzmann constant and T the absolute temperature. About five million MC steps were always performed in order to obtain equilibrium thermodynamical quantities.

In the case of pure copper a crystal with the fcc structure was first set up and the MC simulation performed at 1600 K. The equilibrium structure obtained in this way is a liquid as it should be since copper melts at 1358 K. Starting from this configuration further MC simulation has been carried out at 1200 K. The equilibrium state then represents the supercooled liquid at this temperature and the cohesive energy of this system, equal to 3.19 eV/atom, was then taken as E^{Cu} in Eq. (B1). To obtain E^{rand} the MC simulation was carried out for the block consisting of 78% of copper atoms and 22% of bismuth atoms. The starting configuration was again an fcc structure in which 22% of copper atoms were randomly replaced by bismuth. The equilibrium configuration obtained by the simulation is a disordered liquid, as expect-

ed from the copper-bismuth phase diagram. For the potentials constructed here $E^{\text{rand}}=2.81$ eV in this disordered liquid phase and thus $\Delta H^{\text{mix}}=0.068$ eV. The measured enthalpy of mixing of the liquid copper-bismuth solution at 1200 K is 0.046 ± 0.009 eV/atom.[30] While the match of the calculated and experimental enthalpy of mixing is not exact it is sufficient considering the uncertainties involved in the experimental value.

*On leave from the Institute of Physical Metallurgy, Czechoslovak Academy of Sciences, Žižkova 22, Brno, Czechoslovakia.
†Present address: Fritz-Haber-Institut, Faradayweg 4-6, D-1000 Berlin 33, Germany.
‡Present address: Instituto de Física de Líquidos y Sistemas Biológicos (IFLYSIB), C.C. 565, La Plata (1900), Argentina.

[1]S. S. Hecker, D. L. Rohr, and D. F. Stein, Metall. Trans. A **9**, 481 (1978).
[2]O. Iuzmi and T. Takasugi, J. Mater. Res. **3**, 426 (1988).
[3]C. T. Liu, Scripta. Metall. Mater. **25**, 1231 (1991).
[4]S. F. Pugh, *An Introduction to Grain Boundary Fracture in Metals* (The Institute of Metals, London, 1991).
[5]A. Joshi and D. F. Stein, J. Inst. Metals **99**, 178 (1971).
[6]B. D. Powell and D. P. Woodruff, Philos. Mag. A **34**, 169 (1976).
[7]A. M. Donald and L. M. Brown, Acta Metall. **27**, 59 (1979).
[8]T. G. Ference and R. W. Balluffi, Scripta Metall. **22**, 1929 (1988).
[9]M. Menyhard, B. Blum, and C. J. McMahon Jr., Acta Metall. **37**, 549 (1989).
[10]B. Blum, B. Menyhard, D. E. Luzzi, and J. McMahon C. J., Scripta. Metall. Mater. **24**, 2169 (1990).
[11]M. R. Fitzsimmons and S. L. Sass, Acta Metall. **37**, 1009 (1989).
[12]M. S. Taylor, I. Majid, P. D. Bristowe, and R. W. Balluffi, Phys. Rev. B **40**, 2772 (1989).
[13]D. E. Luzzi, in *Proceedings of the Twelfth International Congress for Electron Microscopy,* edited by L. D. Peachey and D. B. Williams (San Francisco Press, San Francisco, 1990), p. 318.
[14]D. E. Luzzi, Ultramicroscopy **37**, 180 (1991).
[15]U. Dahmen, C. J. D. Hetherington, M. A. O'Keefe, K. H. Westmacott, M. J. Mills, M. S. Daws, and V. Vitek, Philos. Mag. Lett. **62**, 327 (1990).
[16]M. J. Mills and M. S. Daw, in *High Resolution Electron Microscopy of Defects in Materials,* edited by R. Sinclair, D. J. Smith, and U. Dahmen, MRS Symposia Proceedings No. 183 (Materials Research Society, Pittsburgh, 1991), p. 15.
[17]D. E. Luzzi, Min Yan, M. Šob, and V. Vitek, Phys. Rev. Lett. **67**, 1894 (1991).
[18]M. S. Daw and M. I. Baskes, Phys. Rev. B **29**, 6443 (1984).
[19]M. W. Finnis and J. E. Sinclair, Philos. Mag. A **50**, 45 (1984).
[20]A. E. Carlsson, in *Solid State Physics,* edited by H. Ehrenreich and D. Turnbull (Academic, New York, 1990), Vol. 43, p. 1.
[21]E. Tarnow, P. D. Bristowe, J. D. Joannopoulos, and M C. Payne, J. Phys. C **1**, 327 (1989).
[22]R. E. Thomson and D. J. Chadi, Phys. Rev. B **29**, 889 (1984).
[23]A. T. Paxton and A. P. Sutton, Acta Metall. **37**, 1693 (1989).
[24]V. Vitek and J. T. M. DeHosson, in *Computer-Based Microscopic Description of the Structure and Properties of Materials,* edited by J. Broughton, W. Krakow, and S. T. Pantelides, MRS Symposia Proceedings No. 63 (Materials Research Society, Pittsburgh, 1986), p. 125.
[25]S. M. Foiles, Surf. Sci. **191**, 329 (1987).
[26]S. P. Chen and A. F. Voter, Surf. Sci. Lett. **244**, L107 (1991).
[27]G. J. Ackland and V. Vitek, Phys. Rev. B **41**, 10 324 (1990).
[28]A. F. Voter and S. P. Chen, in *Characterization of Defects in Materials,* edited by R. W. Siegel, R. Sinclair, and J. R. Weertman, MRS Symposia Proceedings No. 82 (Materials Research Society, Pittsburgh, 1987), p. 175.
[29]V. Vitek, G. J. Ackland, and J. Cserti, in *Alloy Phase Stability and Design,* edited by G. M. Stocks, D. P. Pope, and A. G. Giamei, MRS Symposia Proceedings No. 186 (Materials Research Society, Pittsburgh, 1991), p. 237.
[30]A. L. Lomov and A. N. Krestovnikov, Izv. Vysshikh Uchebn. Zavedenij, Tsvetnaja Metal. **1**, 84 (1964).
[31]G. J. Ackland, M. W. Finnis, and V. Vitek, J. Phys. F **18**, L153 (1988).
[32]G. J. Ackland, G. Tichy, V. Vitek, and M. W. Finnis, Philos. Mag. A **56**, 735 (1987).
[33]W. B. Pearson, *Handbook of Lattice Spacings and Structures of Metals and Alloys* (Pergamon, Oxford, 1967).
[34]J. Donohue, *The Structure of the Elements* (Wiley, New York, 1973).
[35]G. Simmons and H. Wang, *Single Crystal Elastic Constants and Calculated Aggregate Properties* (M.I.T. Press, Cambridge, MA, 1971).
[36]M. T. Yin and M. L. Cohen, Phys. Rev. B **26**, 5668 (1982).
[37]E. Voce and A. P. C. Hallowes, J. Inst. Metals **73**, 323 (1947).
[38]K. Maeda, V. Vitek, and A. P. Sutton, Acta Metall. **30**, 2001 (1982).
[39]M. Methfessel, Phys. Rev. B **38**, 1537 (1988).
[40]M. Methfessel, C. O. Rodriguez, and O. K. Andersen, Phys. Rev. B **40**, 2009 (1989).
[41]E. C. Urdaneta, D. E. Luzzi, and J. McMahon C. J., in *Structure and Properties of Interfaces in Materials,* edited by W. A. T. Clark, U. Dahmen, and C. L. Briant, MRS Symposia Proceedings No. 238 (Materials Research Society, Pittsburgh, 1992), p. 201.
[42]P. G. Self and M. A. O'Keefe, in *High Resolution Transmission Electron Microscopy and Associated Techniques,* edited by P. R. Buseck, J. M. Cowley, and L. Eyring (Oxford University Press, Oxford, 1988), p. 244.
[43]D. E. Luzzi, Philos. Mag. Lett. **63**, 281 (1991).
[44]*The Structure of Surfaces II,* edited by J. F. Van der Veen and M. A. Van Hove (Springer, Berlin, 1988).
[45]S. P. Chen, A. F. Voter, R. C. Albers, A. M. Boring, and P. J. Hay, J. Mater. Res. **5**, 955 (1990).
[46]L. D. Marks, Ultramicroscopy **18**, 33 (1985).
[47]D. E. Luzzi and L. D. Marks, in *Proceedings of the EMSA,* edited by G. W. Bailey (San Francisco Press, San Francisco, 1987), p. 78.
[48]O. K. Andersen, O. Jepsen, and D. Glötzel, in *Highlights of Condensed Matter Theory,* edited by F. Bassani, F. Fumi, and M. P. Tosi (North Holland, Amsterdam, 1985), p. 59.
[49]O. K. Andersen, O. Jepsen, and M. Šob, in *Electronic Band Structure and Its Applications,* edited by M. Yussouff (Springer, New York, 1987), p. 1.
[50]C. O. Rodriguez, A. I. Liechtenstein, I. I. Mazin, O. Jepsen, O. K. Andersen, and M. Methfessel, Phys. Rev. B **42**, 2692 (1990).
[51]E. S. Machlin, Acta Metall. **22**, 95 (1974).

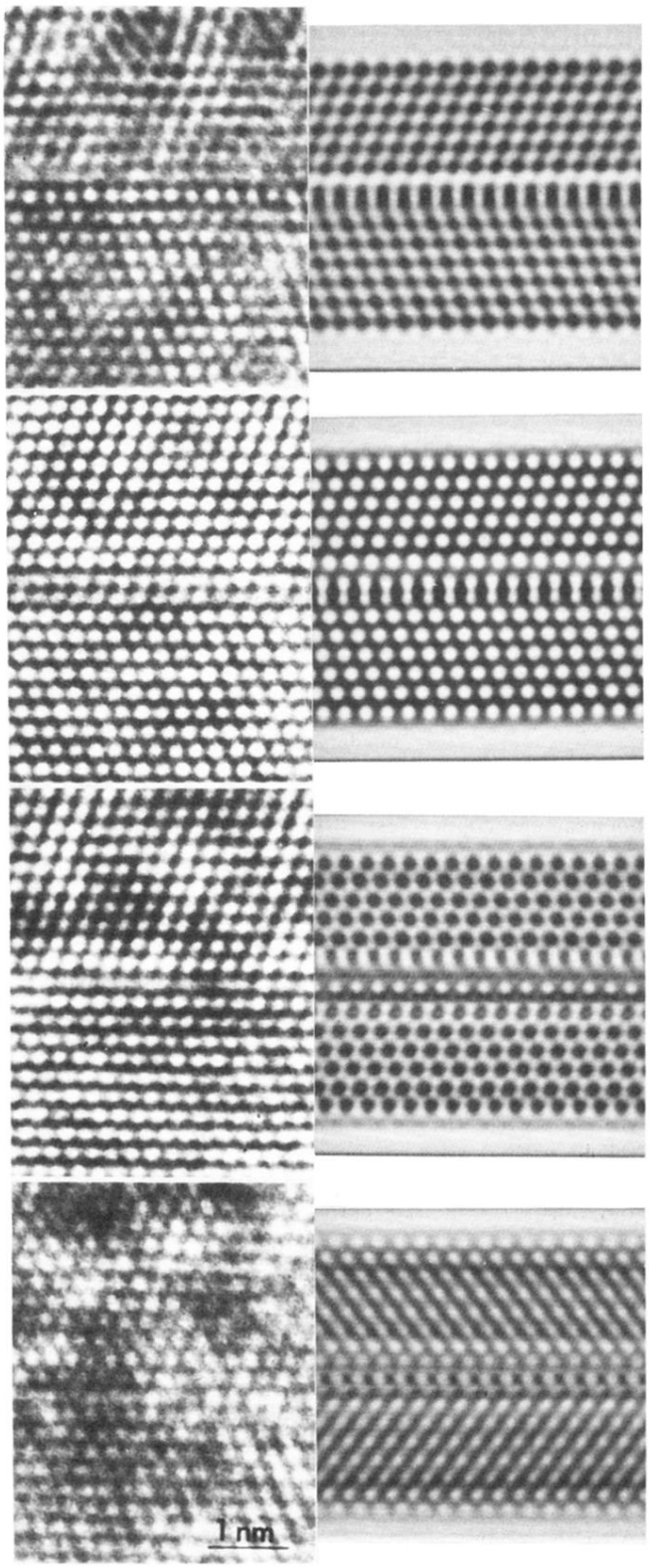

FIG. 4. Experimental (left column) and calculated (right column) image series with objective lens underfocus increasing down the figure. The marker represents 15 Å.